Dominance of misfolded intermediates in the dynamics of α-helix folding

Milo M. Lin[a], Dmitry Shorokhov[b], and Ahmed H. Zewail[b,1]

[a]Pitzer Center for Theoretical Chemistry, University of California, Berkeley, CA 94720; and [b]Physical Biology Center for Ultrafast Science and Technology, Arthur Amos Noyes Laboratory of Chemical Physics, California Institute of Technology, Pasadena, CA 91125

Contributed by Ahmed H. Zewail, August 26, 2014 (sent for review August 1, 2014; reviewed by Martin Gruebele, David J. Wales, and Feng Gai)

Helices are the "hydrogen atoms" of biomolecular complexity; the DNA/RNA double hairpin and protein α-helix ubiquitously form the building blocks of life's constituents at the nanometer scale. Nevertheless, the formation processes of these structures, especially the dynamical pathways and rates, remain challenging to predict and control. Here, we present a general analytical method for constructing dynamical free-energy landscapes of helices. Such landscapes contain information about the thermodynamic stabilities of the possible macromolecular conformations, as well as about the dynamic connectivity, thus enabling the visualization and computation of folding pathways and timescales. We elucidate the methodology using the folding of polyalanine, and demonstrate that its α-helix folding kinetics is dominated by misfolded intermediates. At the physiological temperature of $T = 298$ K and midfolding time $t = 250$ ns, the fraction of structures in the native-state (α-helical) basin equals 22%, which is in good agreement with time-resolved experiments and massively distributed, ensemble-convergent molecular-dynamics simulations. We discuss the prominent role of β-strand–like intermediates in flight toward the native fold, and in relation to the primary conformational change precipitating aggregation in some neurodegenerative diseases.

protein folding | misfolding intermediates

If there is one signature characteristic of biological macromolecules, it is the presence of helices. The double helix is the dominant feature of DNA and RNA, and, in proteins, the α-helix is the most ubiquitous structural motif. The formation and decay of α-helices play a pivotal role in protein folding (and misfolding). Indeed, even for proteins containing little native helical structure, helix formation, concomitant with hydrophobic collapse, seems to be a universal precursor of the folding process (1), much as the nonnative conversion of helical (or disordered) to β-strand–rich structures is the precursor to protein aggregation diseases such as Alzheimer's (2). Although the thermodynamics of such transformations was well understood beginning with the 1950s, the dynamical pathways and rates involved have remained an area of active research. Thus, relatively little was known about the associated kinetics until the end of the 1990s (3). With the advent of temperature-jump (*T*-jump) experimental techniques, the rates of the helix–coil transitions became readily measurable (4–6), whereas the progress in temporal resolution spanning both the nanosecond (7) and picosecond (8) regimes elucidated the early steps of folding/unfolding. Importantly, studies of the elementary steps accompanying such processes can now uncover the nature of kinetic-intermediate states, as well as their characteristic lifetimes (8, 9).

Here, we introduce a statistical mechanical method of constructing dynamical free-energy landscapes of helices. The dynamical landscape allows folding pathways and rates to be visualized and computed in terms of elementary structural steps. For a representative polypeptide with high helix propensity (polyalanine), we construct the dynamical landscape and simulate the folding dynamics using the kinetic-intermediate structure (KIS) model of α-helix elongation. Surprisingly, and in agreement with ensemble-convergent molecular-dynamics (MD) simulations, we find that the α-helix folding timescale and pathways are dominated by misfolded β-hairpin–like kinetic intermediates. These off-pathway misfolded intermediates characterized by nonhelical hydrogen-bonding contacts significantly increase the effective enthalpic folding barrier. The results of the model, which reproduce the measured helix folding rates, are consistent with ensemble-convergent MD simulations, and explain why the measured rates are two orders of magnitude slower than those of the elementary nucleation and elongation steps. The potential importance of these thermodynamically underrepresented kinetic intermediates in folding, misfolding, and aggregation should now be explored in other polypeptides and proteins. In what follows, we discuss the results of the KIS model and provide a comparison with those we obtained using all-atom simulations and experimental studies of α-helix folding/unfolding.

Interestingly, the bifurcation of trajectories (10) and the presence of reactive intermediates (11) found here mirror the behavior in elementary reaction dynamics (11–13). Even in three-atom systems (ABA), it was shown that intermediate structures persist, and their existence accounts for the observed lengthening of the lifetimes involved in the rate process (12, 13). The thermodynamic description in this case misses features of the dynamic energy surface and of course provides neither the extent of bifurcation nor the rates of the involved processes.

Ensemble-Convergent Molecular Dynamics

It is now well established that, due to nonnative structure formation, the so-called "random-coil" (unfolded) state of proteins is neither random nor completely denatured (14). In a similar way, collapsed (but not folded) structures of α-helical proteins may be

Significance

Proteins fill the vast majority of infrastructural and functional roles at the biological nanoscale. Despite their structural variability, most proteins contain α-helix motifs. Aptly described as molecular zippers, α-helices form by first aligning numerous degrees of freedom to stabilize a helical nucleus, after which the helix can presumably rapidly grow. Here, we show that helix zipping in polyalanine can get "caught" by nonhelical contacts that block growth, and that these misfolded intermediates can dominate the folding process, leading to zipping times that are an order of magnitude longer than expected based on unimpeded growth. The dominance of intermediate misfolded structures and their influence on folding dynamics have implications for protein aggregation, which is of significance in diseases such as Alzheimer's.

Author contributions: M.M.L., D.S., and A.H.Z. designed research, performed research, and wrote the paper.

Reviewers: M.G., University of Illinois at Urbana–Champaign; D.J.W., Cambridge University; and F.G., University of Pennsylvania.

The authors declare no conflict of interest.

[1]To whom correspondence should be addressed. Email: zewail@caltech.edu.

This article contains supporting information online at www.pnas.org/lookup/suppl/doi:10.1073/pnas.1416300111/-/DCSupplemental.

stabilized by nonnative hydrogen bonds (15), giving rise to β-hairpin–like moieties (16) and "intramolecular amyloid" motifs (17). To illustrate the effect of protein misfolding, we begin by examining the folding process of alanine polypeptide in aqueous solution, which has long served as the model system for studying α-helix formation. As described in *SI Text*, the MD simulations were carried out, using the CHARMM force field, on the macromolecule solvated in a box of atomistic water and counterions. Care has been taken to ensure the convergence of numerous trajectories ($n = 287$) to represent the behavior of the entire ensemble.

An examination of subpopulations that dominate large ensembles consisting of 25-residue polypeptides of alanine amino acids (A_{25}; Figs. 1 and 2) reveals that α-helical nuclei form within several nanoseconds across the entire macromolecular ensemble, whereas water-mediated structures resembling β-hairpins that appear to encompass a larger fraction of the macromolecule than α-helices during the initial stages of folding control the helix elongation rate. Indeed, because growth of helical islands requires unraveling of misfolded structural motifs that hinder further zipping, the helix elongation process in polyalanine appears to be significantly slower than the helix nucleation process. Moreover, the gradual decay of the β-hairpin population correlates with the rise of helicity fraction across the MD ensemble of A_{25} at longer simulation times (Fig. 2).

Another important observation we made during the course of the ensemble-convergent MD simulations was the predominant validity of the single-sequence approximation (SSA), in which only one helical segment is present at a time within a given polypeptide chain. As evidenced in the results of Fig. 2*A*, the SSA holds for an absolute majority of studied macromolecular structures, which is explained by a significant barrier to nucleating multiple helices during the initial stages of folding. For A_{25}, this barrier may be attributed to the β-hairpin–like misfolded motifs that prevent formation of new α-helical nuclei following the initial nucleation event (Fig. 1). Being an important postulate of the equilibrium and "kinetic zipper" models (5, 18, 19) most commonly used to describe macromolecular transformations, the SSA is also an approximation used in our KIS model of helix–coil transitions in biopolymers such as DNA (20–22) and α-helical polypeptides. Significantly, this makes all of the relevant (partially folded) states of the macromolecule describable by just two variables (i and j; see below). In the following, we take advantage of the SSA to formulate a pictorial model of α-helix elongation and demonstrate that, by properly incorporating the effect of misfolding, the KIS model provides a robust mechanism of the α-helix formation kinetics.

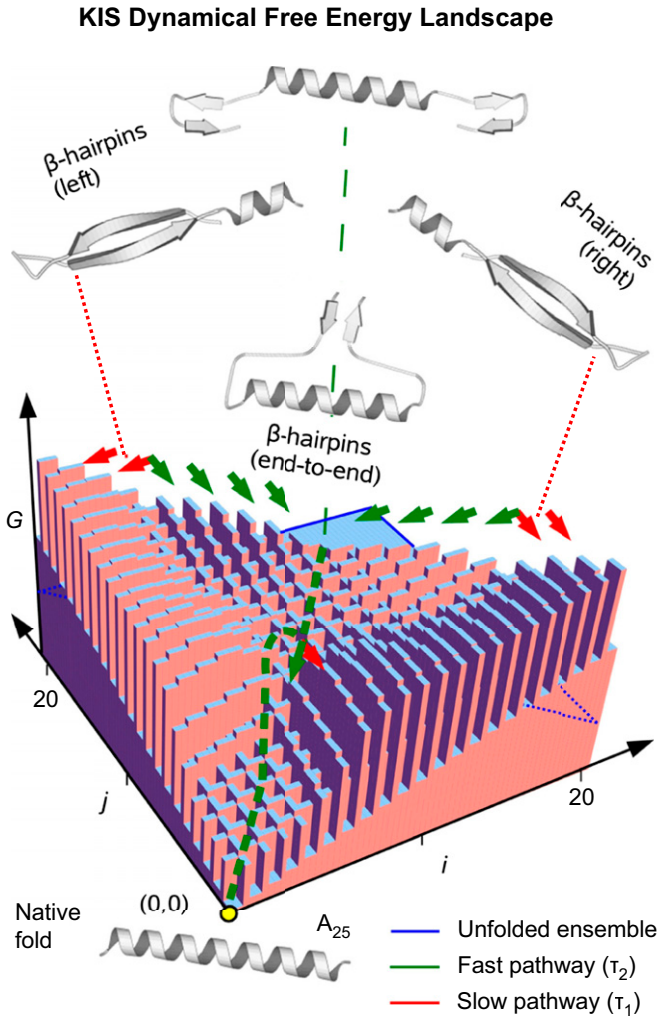

Fig. 1. Folding of A_{25} α-helix. Shown is the free-energy landscape that guides the (un)folding of A_{25} in aqueous solution as obtained from the KIS model at $T = 278$ K. The green dashed line denotes the locus of folding pathways. Reaction coordinates i and j are chosen to be the number of broken ("unzipped") native contacts on the C and N termini of the chain, respectively.

KIS Landscape

In a typical free-energy landscape parameterized by coarse-grained structural coordinates, the conformational space, even for a short polypeptide, contains many more degrees of freedom than can be plotted. The approach to studying the landscape is to either project structural degrees of freedom onto a 1D-or-2D landscape parameterized by coarse-grained coordinates (23, 24), or to dispense with the landscape and represent the relevant states explicitly (e.g., as Markov states) (25, 26). In ref. 26, Wales and colleague have demonstrated the applicability of the latter methodology for polyalanine, and, in this approach, the set of Markov states and the transition rates between the states must be related to relevant conformational structures.

Here, we describe the KIS model for the folding of 1D motifs such as helices, which has the additional property of being "kinetically connected," in that all states that can interconvert via an elementary folding step (i.e., a single helical contact) are neighbors on the grid, and vice versa. All of the microstates in a given state on the "KIS landscape" share the same folded (helical) region of the peptide and can be represented by a single structural motif. Consequently, kinetic connectivity allows for the structural visualization and calculation of kinetic pathways and rates, respectively, once the free-energy landscape is built on this grid. For a polypeptide capable of forming L α-helical hydrogen bonds $\{k \ldots k+4\}$, $k \in [1, L]$, the reaction coordinates $i \in [0, L]$ and $j \in [0, L]$, are chosen to represent the numbers of such bonds that are broken ("unzipped") counting from the C and N termini of the chain, respectively (Fig. S1*A*). We note that the choice of the coordinates implicitly constrains the model to the SSA. All intermediate states are then represented by the unique set of coordinates $\{(i, j)\}$ on the 2D reaction coordinate grid, with the native-fold (α-helical) structure of the protein located at (0, 0). Therefore, every given node (i, j) of the grid corresponds to an ensemble of macromolecular structures that share the same set of intact α-helical hydrogen bonds but may differ in their detailed atomic coordinates, including all possible conformations of the nonhelical moieties of the chain. The only state that is not associated with a unique point on the grid is the "coil" (or completely unfolded ensemble), which is represented by the points on the diagonal boundary of the coordinate space $(i, L - i)$. The KIS free-energy landscape $G(i, j)$ that defines the folding behavior of the macromolecular ensemble is obtained by calculating the

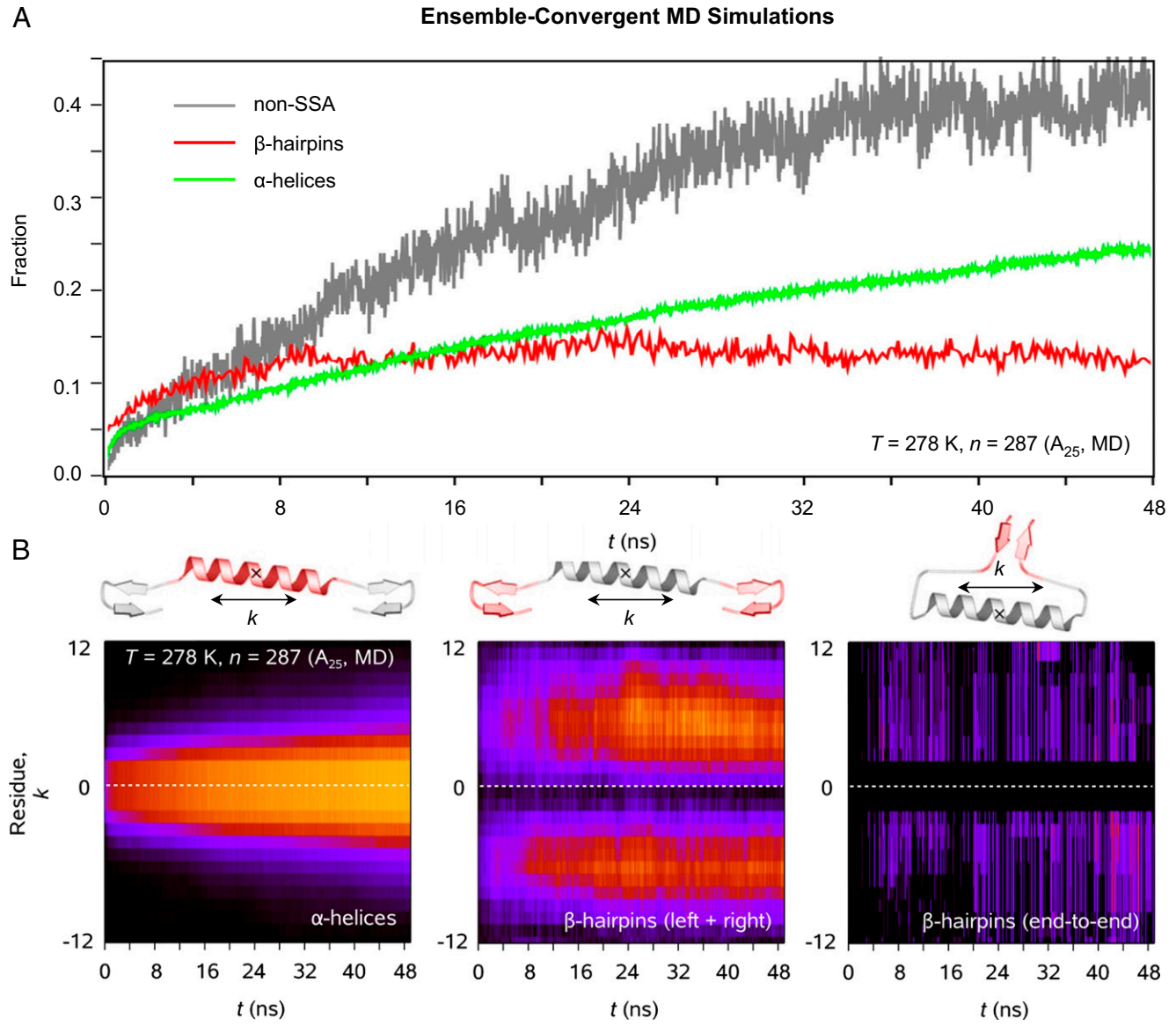

Fig. 2. Ensemble-convergent MD simulations. At $T = 278$ K, the results indicate that rapid formation of α-helical nuclei across the ensemble of A_{25} is followed by severe folding retardation caused by the predominance of misfolded β-hairpin–like structural motifs (*A*). Elongation of α-helical sequences (black, 0%; yellow, 100%) is mostly hindered by formation of long, single-end–capping β-strands ("left + right"; black, 0%; yellow, 16%), with the share of end-to-end contacts being negligible (black, 0%; yellow, 1%). Individual residues k are numbered from –24 to +24 with the center of each helical stretch in the MD ensemble fixed at the origin by definition (*B*); see Fig. S1*C*.

free energy for each (i, j)-state with respect to the unfolded state $(i, L - i)$, as well as the interstate misfolding barriers that are crossed during the course of transitions between neighboring states. The barrier going from (i, j) to $(i - 1, j)$ is equal to the enthalpic penalty of breaking a nonnative hydrogen bond weighted by the probability, over all possible conformations, that position i is occupied by a nonnative bond in state (i, j).

Significantly, although the KIS landscape of A_{25} is only parameterized by the number of broken native hydrogen bonds on either end of the α-helix, the contribution of the entire subensemble of possible misfolded (β-hairpin–type) motifs retarding the folding kinetics is accounted for in the interstate barriers (or roughness) of the landscape. Below, we demonstrate that, in contrast to the behavior exhibited by simple chemical systems, in systems with numerous degrees of conformational freedom the abovementioned roughness can overwhelm the free-energy differences and on-pathway (entropic) barriers between (i, j)-states along folding trajectories (Fig. S1*B*), thereby determining the overall folding behavior and its timescales.

Kinetic Zipper Model

The widely used (27) kinetic zipper—or nucleation-elongation—model (5, 18, 19) of α-helix formation was introduced by Eaton and colleagues in the late 1990s, and lucidly characterizes the on-pathway elementary processes involved. In the model, the nucleation step, which comprises the entropy-dominated conformational search for the correct helical alignment of three sets of consecutive backbone torsional angles, is the slowest step of the helix folding process. Each subsequent "zipping" (or elongation) event, which requires the helical alignment of only one set of torsional angles, proceeds at a relatively faster rate. If these elementary steps are the only ones involved, their cumulative times would determine the helix formation rate. However, depending on the protein sequence, long-lived off-pathway kinetic intermediates

may impede the zipping process. Indeed, helix folding experiments demonstrated that the timescale of the nucleation step could be relatively fast: α-helix nucleation, when observed under no-zipping conditions, occurs on a few-nanosecond timescale, which is consistent with analytical and computational assessments carried out in this (8, 9) and other laboratories (28, 29). In contrast, the overall helix folding timescale at room temperature is broadly distributed depending on sequence, typically being hundreds of nanoseconds (18, 19).

Equally important is the fact that the enthalpic barrier for diffusion-limited helix formation is at most 4 kcal/mol (due to the temperature dependence of the viscosity), whereas the measured barrier is 8 kcal/mol. The discrepancy of ∼4 kcal/mol between on-pathway folding and the experimental evidence cannot be accounted for by mechanisms like, e.g., dipole–dipole interactions (18) and suggests that the elongation process may be more nuanced than one would naïvely expect. Indeed, if the folding barrier were primarily entropic in nature, experimentally measured folding times would likely not differ by several orders of magnitude for α-helical polypeptides of different sequences and similar lengths (30). The above picture suggests that relevant off-pathway interactions besides (native) α-helical contacts can, in fact, comprise the rate-determining step. Therefore, by extending the kinetic zipper framework to the misfolding-dominated regime, the KIS landscape can be used to describe the spectrum of sequence-dependent helix formation mechanisms.

Results and Discussion

Despite being feature-rich, the free-energy landscape of α-helix folding as obtained from the KIS model for A_{25} (Fig. 1) can be characterized by two major domains corresponding to structurally diverse populations: (*i*) misfolded and (*ii*) seminative. The latter, much smaller in size, consists of helices with up to four broken terminal $k \ldots k + 4$ contacts that rapidly zip toward the native fold, whereas the former is shaped by a maze that funnels the helical motifs nucleating close to the middle of the polypeptide chain into the major along-the-diagonal folding locus and, simultaneously, retards those nucleating in the vicinity of the termini of the chain. The macromolecular structures populating the larger basin range from β-hairpin–dominated (and kinetically trapped in the rough $i >> j$ and $j >> i$ subdomains) to long α-helix stretches capped by small misfolded loops ($i \sim j$).

As evidenced in the results of Fig. S2*A*, the former gradually evolve toward the native fold as the β-hairpin stretches are slowly unraveled, which gives rise to a severely misfolded population, whereas the latter need to surmount a relatively low free-energy barrier to proceed with the (fast) end-segment zipping, the height of the barrier being mostly determined by the capping loops. Indeed, the ensemble-averaged helix content as well as the population and location of misfolded structural motifs (Fig. 2*B*) as obtained from our ensemble-convergent MD simulations indicate that single-end–capping hairpins (denoted "left" and "right" in Fig. 1) are significantly more stable and abundant than end-to-end hairpins. We note that, given the roughness of the landscape of Fig. 1, the interconversions between individual microstates must be dominated by unraveling of misfolded-structure motifs off the α-helix reaction pathway rather than conformational diffusion along the pathway.

For coil-to-helix transformation of A_{25} in aqueous solution, ensemble-convergent Monte Carlo simulations of α-helix elongation, starting at random nucleation sites, were performed on the KIS free-energy landscapes at various temperatures. Depicted in Fig. 3 are temporal snapshots of macromolecular-ensemble populations as obtained from KIS–Monte Carlo simulations

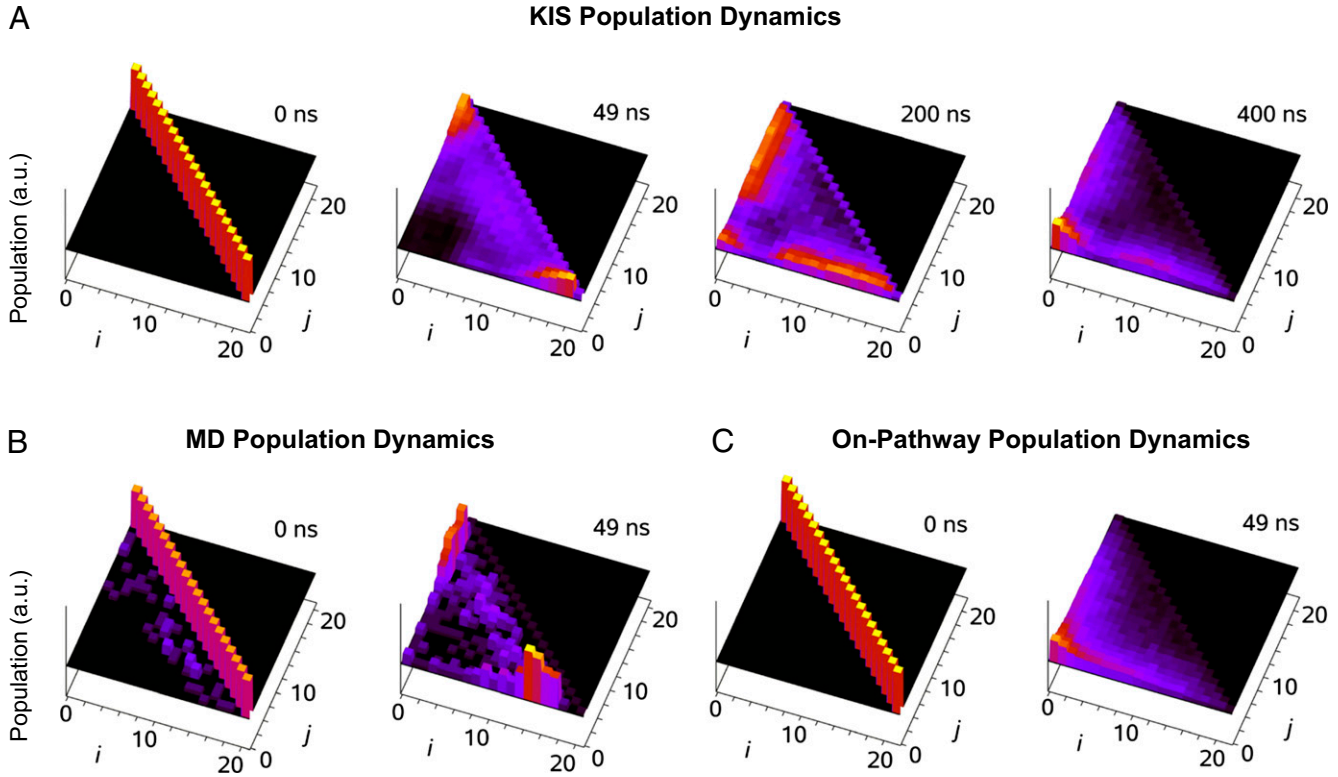

Fig. 3. Misfolded intermediates and population dynamics during α-helix folding. Shown are temporal snapshots of macromolecular ensemble populations of A_{25} at $T = 278$ K as obtained from Monte Carlo dynamics simulations on the KIS free-energy landscape (*A*), which are in good agreement with those obtained from the ensemble-converged MD (*B*). For comparison, also presented is Monte Carlo dynamics in the absence of the misfolding barriers on the KIS free-energy landscape (*C*). See also Movies S1–S4.

carried out at T = 278 K, with and without the free-energy landscape roughness being taken into account. Clearly, the interstate barriers associated with misfolding and loop formation play a dominant role in determining the actual processes involved, as well as their characteristic timescales: Only the KIS landscape that incorporates the interstate barrier contributions from all possible nonnative interactions (Fig. 3*A*) can reproduce the population dynamics of the ensemble-convergent MD simulations (Fig. 3*B*).

At T = 278 K, the macromolecular structures characteristic of $i >> j$ and $j >> i$ misfolded subdomains remain kinetically trapped as they oscillate between (partial) unfolding and refolding on their way to the native (0, 0) state, whereas at T = 298 K, due to the entropy-driven tilting of the underlying free-energy landscape associated with the native hydrogen bonding alone, the $i \sim j$ subdomain becomes accessible to them as well (Fig. S1*D*). As a result, the kinetic flux through the misfolded intermediate states in the A_{25} KIS landscape (Fig. S2*B*) differs radically for the two temperatures. Thus, the increased availability of the $i \sim j$ folding locus at higher temperatures leads to the onset of a (faster) temporal component τ_2 associated with rapid zipping along the diagonal of the landscape (naturally, the slower τ_1 route characteristic of near-the-edge $i >> j$ and $j >> i$ folding pathways is present at all temperatures as it is solely determined by free-energy landscape roughness; Fig. S1*D*).

At T = 278 K, for which the ensemble-averaged fraction of α-helix content nears 100% at equilibrium, the simulations predict a temporal helicity profile characterized by τ_1 = 480 (10) ns (Fig. 4). As stated above, the clear-cut biexponential behavior characteristic of A_{25} at higher temperatures is explained by the bifurcating nature of the free-energy landscape. Indeed, the faster (tens of nanoseconds) temporal component that contributes ~14% of the signal amplitude at T = 298 K appears to stem from the rapid zipping of the inner segments of polypeptide chains, whereas the elongation of terminal helices, which occurs on a much slower timescale, and accounts for ~86% of the signal amplitude, defines the rate-determining step. The "biexponential" folding behavior evidenced in the results of Fig. 4 at higher temperatures evolves into a single exponential at T = 278 K because relative accessibility of the diagonal folding locus (with folding time τ_2) of the KIS landscape exhibits a pronounced temperature dependence (Fig. S2*B*).

The above picture agrees with experimental results (4, 6, 18). Furthermore, the occurrence of hairpin-like intermediates is noted in computational (MD) studies (31, 32). As evidenced in the results of Fig. 4*B*, the folding rates, as obtained from the KIS model for A_{25}, are in remarkably good agreement with the experimental measurements (18). In addition, the effective barrier as obtained from the (quasi-Arrhenius) dependence of folding rates on temperature, 7.9(2) kcal/mol, exhibits a weak variation with the polypeptide chain length and remains consistent over a wide range of temperatures; its value is in excellent agreement with an early experimental estimate of 8 kcal/mol (18). Accordingly, one-half of the barrier height, which cannot be accounted for by on-pathway mechanisms, is associated with the barrier to collective cleavage of nonnative hydrogen bonds that impede the coil-to-helix transition. The effect of misfolding barriers on α-helix formation can be seen in the dramatic dependence of folding timescales on the location of the seeding helical nucleus within the chain (Fig. S2*A*).

There are experiments in the literature that support the presence of intermediates, but here we want to mention the two that elucidate the effect of the initial temperature of an ensemble of macromolecules on their rates. Unlike the normal (Arrhenius-type) behavior, in which the rates typically increase as the temperature increases, for macromolecules with many intermediates on the energy landscape raising the initial temperature (and measuring the rate) for a helical polymer structure or the α-helix

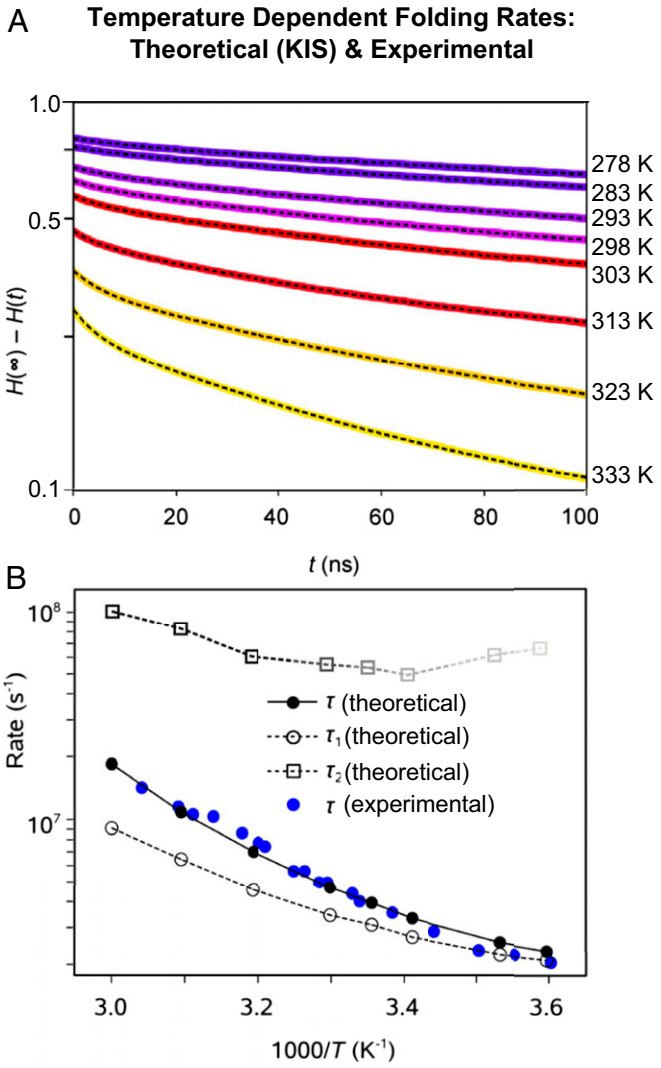

Fig. 4. Folding timescales of A_{25}. Shown is the ensemble-averaged helicity change $H(\infty) - H(t)$ as a function of time, from Monte Carlo dynamics simulated on the KIS landscape (solid lines), and their fits to biexponential kinetics (black dashed lines; *A*). The τ_1 and τ_2 processes give rise to biexponential growth of helicity fraction at physiological temperatures, with the slower timescale in excellent agreement, over a wide temperature range, with that obtained from *T*-jump data of an alanine-rich peptide of comparable length (18). A rapidly decreasing contribution of τ_2 to the overall signal amplitude is depicted with a gray dashed line fading out at lower temperatures (*B*).

refolding results in a slowdown of the relaxation process and hence the decrease in the rates (33, 34).

Conclusion

The most significant concept that emerges from our studies is that α-helix formation is a three-step process involving "helix nucleation," "helix intermediates bottleneck," and "helix zipping." In the bottleneck, trajectories of all collapsed (nonnative) structures that form relatively long-lived misfolded intermediates must be included to obtain the folding rate. Nonnative interactions have long been expected to lead to a slowdown of the folding process. However, here we demonstrate, using the KIS landscape, that the relatively long time of folding in, e.g., polyalanine (A_{25}) can be predicted and compared with ensemble-convergent MD simulations and experimental measurements.

We note that, in the case of α-helix folding of A_{25}, the so-called "conformational diffusion" (35) is rate-limited by misfolding

barriers (roughness of the free-energy landscape), rather than entropy (size of the total conformational space). We also note that for significantly shorter polyalanine chains, such as A_5 (36), the rate is expected to be orders of magnitude faster, reaching the timescale of the initial process, nucleation.

In general, protein folding is governed by the topography (37) of the free-energy landscape (38) and is therefore sequence dependent. The contribution reported here, using the KIS landscape, illuminates the nature of the folding processes characteristic of the basic unit of biological complexity, the α-helix. The important features of the KIS landscape lie in its kinetic connectivity between adjacent states as well as in the inclusion of trajectories originating from the misfolded β-hairpin–like intermediates for the determination of the rates involved. These intermediates may be probed by optical techniques such as nanosecond (39) CD spectroscopy, which enables the measurement of the contribution of the α-helix, β-strand, and random-coil in the ensemble (40).

The timescale and mechanism of β-hairpin involvement in the folding process should be relevant to the primary conformational transition precipitating protein aggregation in diseases such as Alzheimer's. In this case, analogous to A_{25}, β-hairpins are thermodynamically unstable in the population of isolated peptides that are implicated in the disease, both in aqueous solutions (41, 42) and under α-helix–rich membrane-associated (43) conditions. However, antiparallel β-hairpin–like structures (44, 45) have been observed in the aggregated oligomeric state responsible for neurotoxicity (46). This suggests that initiation of the oligomer begins with a misfolded β-hairpin kinetic intermediate that is subsequently thermodynamically stabilized via intermolecular interactions during aggregation. Our results suggest that the fate of a peptide may be determined during the short time window of nonequilibrium folding dynamics following key events such as cleavage of the peptide from its precursor protein, and that the type of rate-limiting misfolded intermediates we describe here are the seeds of oligomerization.

ACKNOWLEDGMENTS. We acknowledge the critical and helpful comments from experts in the field: Drs. William Eaton, Feng Gai, Martin Gruebele, and David Wales. We are grateful to the National Science Foundation for funding of this research. M.M.L. acknowledges financial support from the Krell Institute and the US Department of Energy (US Department of Energy Grant DE-FG02-97ER25308) for a graduate fellowship at Caltech.

1. Roder H (2004) Stepwise helix formation and chain compaction during protein folding. *Proc Natl Acad Sci USA* 101(7):1793–1794.
2. Dobson CM (2008) Protein folding and misfolding: From atoms to organisms. *Physical Biology: From Atoms to Medicine*, ed Zewail AH (Imperial College Press, London), pp 289–335.
3. Muñoz V, ed (2008) *Protein Folding, Misfolding and Aggregation: Classical Themes and Novel Approaches* (RSC, London).
4. Williams S, et al. (1996) Fast events in protein folding: Helix melting and formation in a small peptide. *Biochemistry* 35(3):691–697.
5. Thompson PA, Eaton WA, Hofrichter J (1997) Laser temperature jump study of the helix↔coil kinetics of an alanine peptide interpreted with a "kinetic zipper" model. *Biochemistry* 36(30):9200–9210.
6. Huang CY, Klemke JW, Getahun Z, DeGrado WF, Gai F (2001) Temperature-dependent helix-coil transition of an alanine based peptide. *J Am Chem Soc* 123(38):9235–9238.
7. Ballew RM, Sabelko J, Gruebele M (1996) Direct observation of fast protein folding: The initial collapse of apomyoglobin. *Proc Natl Acad Sci USA* 93(12):5759–5764.
8. Mohammed OF, Jas GS, Lin MM, Zewail AH (2009) Primary peptide folding dynamics observed with ultrafast temperature jump. *Angew Chem Int Ed Engl* 48(31):5628–5632.
9. Lin MM, Mohammed OF, Jas GS, Zewail AH (2011) Speed limit of protein folding evidenced in secondary structure dynamics. *Proc Natl Acad Sci USA* 108(40):16622–16627.
10. Zewail AH (2000) Femtochemistry: Atomic-scale dynamics of the chemical bond using ultrafast lasers. *Angew Chem Int Ed Engl* 39(15):2586–2631.
11. Rose TS, Rosker MJ, Zewail AH (1989) Femtosecond real-time probing of reactions. IV: The reactions of alkali halides. *J Chem Phys* 91(12):7415–7436.
12. Zhong D, Zewail AH (1998) Femtosecond real-time probing of reactions 23: Studies of temporal, velocity, angular, and state dynamics from transition states to final products by femtosecond-resolved mass spectrometry. *J Phys Chem A* 102(23):4031–4058.
13. Møller KB, Zewail AH (1998) Femtosecond dynamics of transition states: The classical saddle-point barrier reactions. *Chem Phys Lett* 295(1):1–10.
14. Lindorff-Larsen K, Piana S, Dror RO, Shaw DE (2011) How fast-folding proteins fold. *Science* 334(6055):517–520.
15. Bertsch RA, Vaidehi N, Chan SI, Goddard WA, 3rd (1998) Kinetic steps for α-helix formation. *Proteins* 33(3):343–357.
16. Mortenson PN, Evans DA, Wales DJ (2002) Energy landscapes of model polyalanines. *J Chem Phys* 117(3):1363–1376.
17. Prigozhin MB, Gruebele M (2011) The fast and the slow: Folding and trapping of $\lambda_{6\text{-}85}$. *J Am Chem Soc* 133(48):19338–19341.
18. Thompson PA, et al. (2000) The helix-coil kinetics of a heteropeptide. *J Phys Chem B* 104(2):378–389.
19. Doshi UR, Muñoz V (2004) The principles of α-helix formation: Explaining complex kinetics with nucleation–elongation theory. *J Phys Chem B* 108(24):8497–8506.
20. Lin MM, Meinhold L, Shorokhov D, Zewail AH (2008) Unfolding and melting of DNA (RNA) hairpins: The concept of structure-specific 2D dynamic landscapes. *Phys Chem Chem Phys* 10(29):4227–4239.
21. Lin MM, Shorokhov D, Zewail AH (2009) Structural ultrafast dynamics of macromolecules: Diffraction of free DNA and effect of hydration. *Phys Chem Chem Phys* 11(45):10619–10632.
22. Crow JM (2008) Computational model reveals how DNA and RNA fold into hairpins: Genetic code does the twist. *Chem Biol* 3(7):B50.
23. Portman JJ, Takada S, Wolynes PG (1998) Variational theory for site resolved protein folding free energy surfaces. *Phys Rev Lett* 81(23):5237–5240.
24. Portman JJ, Takada S, Wolynes PG (2001) Microscopic theory of protein folding rates. I. Fine structure of the free energy profile and folding routes from a variational approach. *J Chem Phys* 114(11):5069–5081.
25. Noé F, Schütte C, Vanden-Eijnden E, Reich L, Weikl TR (2009) Constructing the equilibrium ensemble of folding pathways from short off-equilibrium simulations. *Proc Natl Acad Sci USA* 106(45):19011–19016.
26. Mortenson PN, Wales DJ (2001) Energy landscapes, global optimization and dynamics of the polyalanine $Ac(ala)_8NHMe$. *J Chem Phys* 114(14):6443–6454.
27. Ferguson N, Fersht AR (2003) Early events in protein folding. *Curr Opin Struct Biol* 13(1):75–81.
28. Tobias DJ, Mertz JE, Brooks CL, 3rd (1991) Nanosecond time scale folding dynamics of a pentapeptide in water. *Biochemistry* 30(24):6054–6058.
29. Hummer G, García AE, Garde S (2001) Helix nucleation kinetics from molecular simulations in explicit solvent. *Proteins* 42(1):77–84.
30. Doshi UR (2008) Kinetics and mechanisms of α-helix formation. *Protein Folding, Misfolding and Aggregation: Classical Themes and Novel Approaches*, ed Muñoz V (RSC, London), pp 35–36.
31. Voegler Smith A, Hall CK (2001) α-Helix formation: Discontinuous molecular dynamics on an intermediate-resolution protein model. *Proteins* 44(3):344–360.
32. Chowdhury S, Zhang W, Wu C, Xiong G, Duan Y (2003) Breaking non-native hydrophobic clusters is the rate-limiting step in the folding of an alanine-based peptide. *Biopolymers* 68(1):63–75.
33. Huang CY, et al. (2002) Helix formation via conformation diffusion search. *Proc Natl Acad Sci USA* 99(5):2788–2793.
34. Kwon O-H, Ortalan V, Zewail AH (2011) Macromolecular structural dynamics visualized by pulsed dose control in 4D electron microscopy. *Proc Natl Acad Sci USA* 108(15):6026–6031.
35. Sorin EJ, Pande VS (2005) Exploring the helix-coil transition via all-atom equilibrium ensemble simulations. *Biophys J* 88(4):2472–2493.
36. De Sancho D, Best RB (2011) What is the time scale for α-helix nucleation? *J Am Chem Soc* 133(17):6809–6816.
37. Wales DJ (2003) *Energy Landscapes with Applications to Clusters, Biomolecules and Glasses* (Cambridge Univ Press, Cambridge, UK).
38. Bryngelson JD, Onuchic JN, Socci ND, Wolynes PG (1995) Funnels, pathways, and the energy landscape of protein folding: A synthesis. *Proteins* 21(3):167–195.
39. Björling SC, Goldbeck RA, Paquette SJ, Milder SJ, Kliger DS (1996) Allosteric intermediates in hemoglobin. 1. Nanosecond time-resolved circular dichroism spectroscopy. *Biochemistry* 35(26):8619–8627.
40. Sreerama N, Venyaminov SY, Woody RW (1999) Estimation of the number of α-helical and β-strand segments in proteins using circular dichroism spectroscopy. *Protein Sci* 8(2):370–380.
41. Lin YS, Pande VS (2012) Effects of familial mutations on the monomer structure of $A\beta_{42}$. *Biophys J* 103(12):L47–L49.
42. Ball KA, et al. (2011) Homogeneous and heterogeneous tertiary structure ensembles of amyloid-β peptides. *Biochemistry* 50(35):7612–7628.
43. Sticht H, et al. (1995) Structure of amyloid A4-(1-40)-peptide of Alzheimer's disease. *Eur J Biochem* 233(1):293–298.
44. Cerf E, et al. (2009) Antiparallel β-sheet: A signature structure of the oligomeric amyloid β-peptide. *Biochem J* 421(3):415–423.
45. Hoyer W, Grönwall C, Jonsson A, Ståhl S, Härd T (2008) Stabilization of a β-hairpin in monomeric Alzheimer's amyloid-β peptide inhibits amyloid formation. *Proc Natl Acad Sci USA* 105(13):5099–5104.
46. Shankar GM, et al. (2008) Amyloid-β protein dimers isolated directly from Alzheimer's brains impair synaptic plasticity and memory. *Nat Med* 14(8):837–842.